Nuclear Density Functional Theory and the Equation of State

Yeunhwan Lim*

Department of Physics and Astronomy

The State University of New York at Stony Brook, Stony Brook, NY, 11790

arXiv:1104.1194v1 [nucl-th] 6 Apr 2011

Abstract

A nuclear density functional can be used to find the binding energy and shell structure of nuclei and the energy gap in superconducting nuclear matter. In this paper, we study the possible application of a nuclear density functional theory to nuclear astrophysics. From energy density functional theory, we can deduce the interaction between nucleons to find a rough estimate of the charge radius of the specific nuclei. Compared to the Finite-Range Thomas Fermi model, we include three-body forces, which might be important at densities several times that of nuclear matter density. We also add the momentum dependent interaction to take into account the effective mass of the nucleons. We study matter in the neutron star crust using the Wigner-Seitz cell method. By constructing the mass-radius relation of neutron stars and investigating lepton-rich nuclear matter in proto-neutron stars, we find that the density functional can be used to construct an equation of state of hot dense matter.

*Electronic address: ylim@mail.astro.sunysb.edu

I. INTRODUCTION

Understanding the equation of state (EOS) of dense matter is important to understand heavy-ion collision, supernova explosions, and neutron stars. Neutron stars are believed to be composed of an outer crust, an inner crust, an outer core, and an inner core. The outer crust ($10^4 \leq \rho \leq 10^{11}\,\mathrm{g\ cm^{-3}}$) has a lattice of neutron-rich nuclei in a gas of free electrons. In the inner crust ($10^{11} \leq \rho \leq 10^{14}\,\mathrm{g\ cm^{-3}}$), there are neutron-rich nuclei in a gas of free electrons and neutrons. The density of the outer core extends to $\sim 5 \times 10^{14}\,\mathrm{g\ cm^{-3}}$ and is a homogeneous liquid mainly composed of neutrons, electrons, protons and muons. Not much is not known about the inner core ($5 \sim 10\rho_0$, where the saturation density is $\rho_0 = 0.16\mathrm{fm}^{-3}$), however, we believe that there are hyperons in the hadronic phase and deconfined quark matter[24]. A proper EOS should be able to explain nuclear properties in all density ranges. We can get basic information about nuclear matter from semiempirical mass formulas. One such fomula, known as the Liquid Drop Model (LDM), determines the binding energy(B) of nuclei in terms of a nuclear matter contribution and various corrections for finite nuclei[5]:

$$B(A) = a_{\mathrm{vol}}A + a_{\mathrm{surf}}A^{2/3} + a_{\mathrm{coul}}Z^2A^{-1/3} + a_{\mathrm{sym}}\frac{(N-Z)^2}{A}\,, \tag{1}$$

where $a_{\mathrm{vol}} \approx -16\mathrm{MeV}$, $a_{\mathrm{surf}} \approx 20\mathrm{MeV}$, $a_{\mathrm{coul}} \approx 0.751\mathrm{MeV}$, $a_{\mathrm{sym}} \approx 21.4\mathrm{MeV}$, N is the number of neutrons, Z is the number of protons, and A is the total number of nucleons in a nucleus[5]. First is the volume term, which is the binding energy of infinite nuclear matter. The second term indicates the reduction of binding due to the nucleons on the surface. The third term represents the Coulomb energy, which is assumed to be that of uniformly-distributed charge. The last term is the symmetry energy, representing the decrease in binding energy for unequal numbers of protons and neutrons.

Baym, Bethe, and Pethick (BBP)[26] made an EOS in the range of densities from $4.3 \times 10^{11}\mathrm{g/cm^3}$, where neutrons begin to drip out of the neuclei, to $5 \times 10^{14}\mathrm{g/cm^3}$ ($2\rho_0$) using a compressible LDM designed to take into account three important features: (i) the free neutron gas due to neutron drip; (ii) the nuclear surface energy reduced by the neutron gas; and (iii) the effect of the nuclear lattice Coulomb energy. Baym, Pethick, and Sutherland[27] extended the previous model in the regime from $10^4\mathrm{g/cm^3}$ to neutron drip and applied it to neutron stars and white dwarfs.

Oyamatsu[25] studied nuclear shapes and lattice types (spherical, cylindrical, slab, cylindricl

hole and spherical hole nuclei) at T = 0 MeV with parametrized neutron and proton distributions, and performed the Thomas-Fermi calculations with four different energy-density functionals. Negele and Vautherin[28] used a different method (Hartree-Fock approximation) to study the equation of state at T = 0 MeV. They were able to get a density-dependent Hamiltonian from two-body interactions and found results similar to BBP.

There were several efforts to make thermodynamic tables that can be used for supernova simulations. One of them is the Lattimer-Swesty EOS (LS)[3]. Their equation of state is an extension of the previous work by Lattimer et al.(LLPR) [4]. The LLPR EOS is based on the LDM. They included the effect of temperature on nuclei, the increase of surface energy as temperature increases, the effect of external nucleons, and the effect of nuclear excited states. The LS EOS also took into account nuclear deformation and the phase transitions from nuclei to uniform nuclear matter at subnuclear densities. Another table was given by Shen et al.[30], in which they used the field-theoretical model with the Thomas-Fermi method. They constructed an EOS of nuclear matter in a wide range of the baryon mass density ($\rho_B = 1.25 \times 10^5 - 2.5 \times 10^{15}$ g/cm^3), temperature ($T = 0 - 100$ MeV), and proton fraction ($Yp = 0 - 0.56$).

Recently, Shen et al.[31] used a density-dependent relativistic mean-field theory to construct a nuclear EOS. For high- and intermediate-density nuclear matter, they employed relativisitic mean field calculations and used the virial expansion to study low-density nuclear matter. The table has the range of density from $\rho_B = 10^{-8} - 1.6\text{fm}^{-3}$, proton fraction $\text{Y}_p = 0 - 0.56$, and temperature $T = 0.16 - 15.8$MeV for high and low density nuclear matter.

In this paper we use a simple density functional model to decribe both high and low nuclear density. To account for the short range of nuclear forces, we use a Gaussian form for the interaction. To find the minimum energy of a nuclear system, we use the Lagrange multiplier method; that is, the chemical potentials of neutrons and protons are constant in the cells of nuclear systems. Using this method, we can find the properties of single nuclei and heavy nuclei with a neutron gas in the neutron star crust. The MIT bag model is used to see the phase transition at high baryon density ($\rho_B > \rho_0$). The mass-radius relation and the moment of inertia of cold neutron stars are calculated using the nuclear density functional. Proto-neutron star matter with neutrinos is also investigated for a given entropy per baryon.

II. NUCLEAR DENSITY FUNCTIONAL THEORY

A. Energy density functional

The energy of the nuclear matter can be given by

$$E = T_{kin} + E_{FR} + E_{ZR} + E_C + E_{S,L} \tag{2}$$

where T_{kin}, E_{FR}, E_{ZR}, E_C, and $E_{S,L}$ are the kinetic energy, nuclear finite-range interaction, zero-range interaction, Coulomb interaction, and spin-orbit coupling respectively. The kinetic energy contribution from nucleons is simply obtained by

$$T_{kin} = \int d^3r \sum_t \frac{\hbar^2}{2m}\tau_t \,, \tag{3}$$

where t is the type of nucleons.

In this Gaussian nuclear density functional (GNDF) theory, the number and kinetic densities are

$$\rho_t = \frac{1}{4\pi^3\hbar^3}\int_0^\infty f_t \, d^3p \,; \quad \tau_t = \frac{1}{4\pi^3\hbar^5}\int_0^\infty f_t p^2 \, d^3p \,, \tag{4}$$

where f_t is the Fermi-Dirac density function,

$$f_t = \frac{1}{1+e^{(\epsilon_t-\mu_t)/T}} \,. \tag{5}$$

For the finite-range term, we use a Gaussian phenomenological model for the nuclear potential,

$$\begin{aligned} E_{FR} = &\sum_t \frac{1}{\pi^{3/2}r_0^3}\int d^3r_1 d^3r_2 e^{-r_{12}^2/r_0^2}\left[V_{1L}\rho_t(\vec{r}_1)\rho_t(\vec{r}_2) + V_{1U}\rho_t(\vec{r}_1)\rho_{t'}(\vec{r}_2)\right] \\ &+ \sum_t \frac{1}{\pi^{3/2}r_0^3}\int d^3r_1 d^3r_2 e^{-r_{12}^2/r_0^2}\left[V_{2L}\rho_t^{1+\epsilon}(\vec{r}_1)\rho_t^{1+\epsilon}(\vec{r}_2) + V_{2U}\rho_t^{1+\epsilon}(\vec{r}_1)\rho_{t'}^{1+\epsilon}(\vec{r}_2)\right] \\ &+ \sum_t \frac{1}{\pi^{3/2}r_0^3}\int d^3r_1 d^3r_2 e^{-r_{12}^2/r_0^2}\left[\int d^3p_{t1} d^3p_{t2} f_{t1} f_{t2} V_{3L} p_{12}^2 + \int d^3p_{t1} d^3p_{t'2} f_{t1} f_{t'2} V_{3U} p_{12}^2\right], \end{aligned} \tag{6}$$

where $p_{12} = |\vec{p}_1 - \vec{p}_2|$, $r_{12} = |\vec{r}_1 - \vec{r}_2|$, r_0 is the length of interaction, and V_{1L}, V_{1U}, V_{2L}, V_{2U}, V_{3L}, and V_{3U} are interaction parameters to be determined. The last term is added to explain the effective mass of nucleons in dense matter.

The zero-range term in the nuclear force can be regarded as the energy contribution from three-body nuclear forces. The three-body force is quite important if the baryon density

increases beyond two or three times the saturation density. One possible form of the three-body force is[5]

$$E_{ZR} = \frac{1}{4} t_3 \int d^3 r \rho_n(r) \rho_p(r) \rho(r) \,, \tag{7}$$

where t_3 is the interaction strength for three-body force, ρ_n (ρ_p) is neutron(proton) density, and ρ is total density.

The energy functional for the Coulomb interaction has an exchange term which is absent in classical physics,

$$\begin{aligned} E_C &= E_C^{pp} + E_C^{ex} \\ &= \frac{e^2}{2} \int \int d^3 r_1 d^3 r_2 \frac{\rho_p(r_1)\rho_p(r_2)}{r_{12}} - \frac{3}{4\pi} (3\pi^2)^{1/3} e^2 \int d^3 r \rho_p^{4/3}(r) \,. \end{aligned} \tag{8}$$

In bulk nuclear matter, the spin-orbit and Coulomb interactions constitute a small portion of the total energy, so we neglect these two terms in bulk nuclear matter. Then the bulk density functional would be

$$\begin{aligned} E_B &= T_{kin} + E_{FR} + E_{ZR} \\ &= \int d^3 r \mathcal{E}_B(r) \,, \end{aligned} \tag{9}$$

where $\mathcal{E}_B$ is the energy density for bulk matter. Using eq. (3), (6), and (7), we find

$$\begin{aligned} \mathcal{E}_B = & \frac{\hbar^2 \tau_n}{2m} + \frac{\hbar^2 \tau_p}{2m} \\ & + V_{1L}(\rho_n \langle \rho_n \rangle + \rho_p \langle \rho_p \rangle) + V_{1U}(\rho_n \langle \rho_p \rangle + \rho_p \langle \rho_n \rangle) \\ & + V_{2L}(\rho_n^{1+\epsilon} \langle \rho_n^{1+\epsilon} \rangle + \rho_p^{1+\epsilon} \langle \rho_p^{1+\epsilon} \rangle) + V_{2U}(\rho_n^{1+\epsilon} \langle \rho_p^{1+\epsilon} \rangle + \rho_p^{1+\epsilon} \langle \rho_n^{1+\epsilon} \rangle) \\ & + V_{3L}(\rho_n \langle \tau_n \rangle + \tau_n \langle \rho_n \rangle + \rho_p \langle \tau_p \rangle + \tau_p \langle \rho_p \rangle) + V_{3U}(\rho_n \langle \tau_p \rangle + \tau_n \langle \rho_p \rangle + \rho_p \langle \tau_n \rangle + \tau_p \langle \rho_n \rangle) \\ & + \frac{1}{4} t_3 \rho \rho_n \rho_p \end{aligned} \tag{10}$$

where we defined the Gaussian-type integral using '$\langle ... \rangle$':

$$\langle u(r_1) \rangle = \frac{1}{\pi^{3/2} r_0^3} \int d^3 r_2 e^{-r_{12}^2/r_0^2} u(r_2) \,. \tag{11}$$

B. Effective mass, potential, and thermodynamic properties

The effective mass of nucleons at the nuclear saturation density is about $0.7 m_B (m_B = 938)$MeV. Some nuclear density functionals use the effective mass $m^* = m_B$; we, however,

introduced the momentum-dependent interaction, which describes the effective mass of nucleons. The functional derivative δE_B gives us the effective masses and potentials in the nuclear density functional,

$$\delta E_B = \int d^3r \left(V_n \delta\rho_n + \frac{\hbar^2}{2m_n^*}\delta\tau_n + V_p\delta\rho_p + \frac{\hbar^2}{2m_p^*}\delta\tau_p \right). \tag{12}$$

Now we get the effective mass for neutrons and protons,

$$m_t^* = \frac{m}{1 + 4m(V_{3L}\langle\rho_t\rangle + V_{3U}\langle\rho_{t'}\rangle)/\hbar^2} \tag{13}$$

and the potentials,

$$\begin{aligned} V_t =& 2\Big[V_{1L}\langle\rho_t\rangle + V_{1U}\langle\rho_{t'}\rangle + (1+\epsilon)\rho_t^\epsilon (V_{2L}\langle\rho_t^{1+\epsilon}\rangle + V_{2U}\langle\rho_{t'}^{1+\epsilon}\rangle) + V_{3L}\langle\tau_t\rangle + V_{3U}\langle\tau_{t'}\rangle \Big] \\ &+ \frac{1}{4}t_3(2\rho_t + \rho_{t'})\rho_{t'} \,. \end{aligned} \tag{14}$$

where t' is a different type of nucleon from t nucleon.

The thermodynamic properties are extremely important for describing the properties of hot, dense matter. The degeneracy parameter in the Fermi-Dirac distribution function is the key to the thermodynamic properties. Using Fermi-integrals, we get the baryon number density and kinetic density in terms of the degeneracy parameter $\phi_t = (\mu_t - V_t)/T$,

$$\rho_t = \frac{1}{2\pi^2}\left(\frac{2m_t^*T}{\hbar^2}\right)^{3/2} F_{1/2}(\phi_t), \quad \tau_t = \frac{1}{2\pi^2}\left(\frac{2m_t^*T}{\hbar^2}\right)^{5/2} F_{3/2}(\phi_t) \,. \tag{15}$$

Landau's quasi-particle formula gives us the entropy density S_t, which tells us how to find the pressure in this density functional,

$$S_t = -\frac{2}{\hbar^3}\int d^3p \big[f_t \ln f_t + (1-f_t)\ln(1-f_t) \big] = \frac{5\hbar^2}{6m_t^*T}\tau_t - \frac{\mu_t - V_t}{T}\rho_t \,. \tag{16}$$

From the thermodynamic identity and entropy density given above, we can get the pressure:

$$\begin{aligned} p &= \mu_n\rho_n + \mu_p\rho_p + TS_n + TS_p - \mathcal{E} \\ &= \sum_t \left(\frac{5\hbar^2}{6m_t^*}\tau_t + V_t\rho_t \right) - \mathcal{E} \\ &= \frac{\hbar^2\tau_n}{3m} + \frac{\hbar^2\tau_p}{3m} + V_{1L}(\rho_n\langle\rho_n\rangle + \rho_p\langle\rho_p\rangle) + V_{1U}(\rho_n\langle\rho_p\rangle + \rho_p\langle\rho_n\rangle) \\ &\quad + V_{2L}(1+2\epsilon)(\rho_n^{1+\epsilon}\langle\rho_n^{1+\epsilon}\rangle + \rho_p^{1+\epsilon}\langle\rho_p^{1+\epsilon}\rangle) + V_{2U}(1+2\epsilon)(\rho_n^{1+\epsilon}\langle\rho_p^{1+\epsilon}\rangle + \rho_p^{1+\epsilon}\langle\rho_n^{1+\epsilon}\rangle) \\ &\quad + V_{3L}(\rho_n\langle\tau_n\rangle + \frac{7}{3}\tau_n\langle\rho_n\rangle + \rho_p\langle\tau_p\rangle + \frac{7}{3}\tau_p\langle\rho_p\rangle) + V_{3U}(\rho_n\langle\tau_p\rangle + \frac{7}{3}\tau_n\langle\rho_p\rangle + \rho_p\langle\tau_n\rangle + \frac{7}{3}\tau_p\langle\rho_n\rangle) \\ &\quad + \frac{1}{2}t_3\rho\rho_n\rho_p \,, \end{aligned} \tag{17}$$

where in zero-temperature, non-uniform matter, the chemical potential of the protons and neutrons are given by,

$$\begin{aligned}\mu_t &= \frac{\hbar^2}{2m_t^*}(3\pi^2\rho_t)^{2/3} + V_t \\ &= \frac{\hbar^2}{2m}(3\pi^2\rho_t)^{2/3} + 2(V_{3L}\langle\rho_t\rangle + V_{3U}\langle\rho_{t'}\rangle)(3\pi^2\rho_t)^{2/3} \\ &\quad + 2\Big[V_{1L}\langle\rho_t\rangle + V_{1U}\langle\rho_{t'}\rangle + (1+\epsilon)\rho_t^{\epsilon}(V_{2L}\langle\rho_t^{1+\epsilon}\rangle + V_{2U}\langle\rho_{t'}^{1+\epsilon}\rangle) + V_{3L}\langle\tau_t\rangle + V_{3U}\langle\tau_{t'}\rangle\Big] \\ &\quad + \frac{1}{4}t_3(2\rho_t + \rho_{t'})\rho_{t'}\,.\end{aligned} \tag{18}$$

III. PARAMETERS FOR THE GAUSSIAN NUCLEAR DENSITY FUNCTIONAL

Every nuclear model should reproduce five nuclear matter properties: binging energy, pressure, nuclear incompressibility, symmetry energy and effective mass, m^*. We use the saturation properties of nuclear matter to determine the parameters of the density functional. For zero-temperature, uniform nuclear matter, we have the energy density as a function of $u = \rho/\rho_0$ and $x = \rho_p/\rho$,

$$\begin{aligned}\frac{\mathcal{E}_B}{T_0\rho_0} &= \frac{3}{5}2^{2/3}u^{5/3}\big[(1-x)^{5/3} + x^{5/3}\big] + u^2\big[v_{1L}(x^2 + (1-x)^2) + 2v_{1U}x(1-x)\big] \\ &\quad + 2^{1+2\epsilon}u^{2+2\epsilon}\big[v_{2L}(x^{2+2\epsilon} + (1-x)^{2+2\epsilon}) + 2v_{2U}x^{1+\epsilon}(1-x)^{1+\epsilon}\big] \\ &\quad + 2^{2/3}u^{8/3}\big[v_{3L}(x^{8/3} + (1-x)^{8/3}) + v_{3U}(x(1-x)^{5/3} + x^{5/3}(1-x))\big] + \frac{1}{4}t_3'u^3x(1-x)\,,\end{aligned} \tag{19}$$

where we define the parameters

$$\begin{aligned}&T_0 = \frac{\hbar^2}{2m}(3\pi^2\rho_0/2)^{3/2}\,, \quad v_{1L,U} = \frac{\rho_0}{T_0}V_{1L,U}\,, \quad v_{2L,U} = \frac{1}{T_0}\Big(\frac{\rho_0}{2}\Big)^{1+2\epsilon}V_{2L,U} \\ &v_{3L,U} = \frac{4\cdot 3^{5/3}\pi^{4/3}}{5T_0}\Big(\frac{\rho_0}{2}\Big)^{5/3}V_{3L,U}\,, \quad t_3' = \frac{\rho_0^2}{T_0}t_3\,.\end{aligned} \tag{20}$$

Now we assume that the momentum-dependent interaction is blind to the type of nucleon, so $V_{3L} = V_{3U}(v_3 = v_{3L} + v_{3U})$. The binding enery of symmetric nuclear matter ($u = 1$, $x = 1/2$) is then given by

$$\frac{\mathcal{E}_0}{\rho_0} = -B_0 = T_0\left[\frac{3}{5} + \frac{v_{1L} + v_{1U}}{2} + v_{2L} + v_{2U} + \frac{v_3}{2} + \frac{t_3'}{16}\right], \tag{21}$$

where $B_0 = 16\text{MeV}$ is the binding energy per baryon at the nuclear saturation density. The pressure at the saturation density vanishes, which mean the enery per baryon has its minimum at the saturation density,

$$p_0 = \rho_0 T_0 \left[\frac{2}{5} + \frac{v_{1L} + v_{1U}}{2} + (1+2\epsilon)(v_{2L} + v_{2U}) + \frac{5}{6} v_3 + \frac{1}{8} t_3' \right] = 0 \,. \tag{22}$$

The incompressibility parameter at the saturation density is given by

$$\begin{aligned} K_0 = 9 \frac{dp}{d\rho}\bigg|_{\rho=\rho_0} &= T_0 \big[6 + 9(v_{1L} + v_{1U}) + 9(1+2\epsilon)(2+2\epsilon)(v_{2L} + v_{2U}) + 20 v_3 + \frac{27}{8} t_3' \big] \\ &= 265\text{MeV} \,. \end{aligned} \tag{23}$$

The symmetry energy in nuclear matter is defined as

$$\begin{aligned} S_v &= \frac{1}{8} \frac{d^2(\mathcal{E}/\rho)}{dx^2}\bigg|_{\rho=\rho_0, x=1/2} \\ &= T_0 \left[\frac{1}{3} + \frac{v_{1L} - v_{1U}}{2} + (1+\epsilon)((1+2\epsilon) v_{2L} - v_{2U}) + \frac{5}{18} v_3 - \frac{1}{16} t_3' \right] \\ &= 28\text{MeV} \,. \end{aligned} \tag{24}$$

Another parameter, which is related to symmetry energy, is given by

$$\begin{aligned} L &= \frac{3\rho_0}{8} \frac{d^3(\mathcal{E}/\rho)}{d\rho dx^2}\bigg|_{\rho=\rho_0, x=1/2} \\ &= T_0 \left[\frac{2}{3} + \frac{3}{2}(v_{1L} - v_{1U}) + 3(1+2\epsilon)(1+\epsilon)((1+2\epsilon) v_{2L} - v_{2U}) + \frac{25}{18} v_3 - \frac{3}{8} t_3' \right] \\ &= 54\text{MeV} \,. \end{aligned} \tag{25}$$

We choose the effective mass at the saturation density as $0.78 m_b$ and use this number in the eq. (13) :

$$m^* = \frac{m}{1 + 2m\rho_0 V_3/\hbar^2} = 0.78 m_b \,. \tag{26}$$

Thus we can easily recover v_3 from eq. (20). From eq. (21), (22), and (23), we can have $v_1 = v_{1L} + v_{2L}$, $v_2 = v_{2L} + v_{2U}$ and t_3'.

$$\begin{aligned} v_1 &= \frac{5K_0/T_0 + 5v_3(1-3\epsilon) - 72\epsilon - 90B_0/T_0(1+2\epsilon) - 12}{45\epsilon} \\ v_2 &= \frac{12 + 90B_0/T_0 - 5K_0/T_0 - 5v_3}{90\epsilon(1-2\epsilon)} \\ t_3' &= -8v_1 - 16v_2 - 8v_3 - \frac{16B_0}{T_0} - \frac{48}{5} \,. \end{aligned} \tag{27}$$

TABLE I: Interaction parameters when $\epsilon = 1/6$, $K = 265$ MeV, $S_v = 28$MeV, $L = 54$MeV.

v_{1L}	v_{1U}	v_{2L}	v_{2U}	$v_{3L,U}$	t_3'	r_0 (fm)
-1.766	-3.472	0.410	0.931	0.169	1.177	1.205

Then we can manipulate eq. (24), and (25) to get v_{1L} and v_{2L},

$$\begin{aligned} v_{1L} &= \frac{1}{2}v_1 + \frac{1}{2\epsilon}\left[\frac{5(1-3\epsilon)}{27}v_3 + \frac{2\epsilon-1}{16}t_3' + \frac{(1+2\epsilon)S_v}{T_0} - \frac{L}{3T_0} - \frac{1+6\epsilon}{9}\right] \\ v_{2L} &= \frac{1}{2(1+\epsilon)}v_2 - \frac{1}{4\epsilon(1+\epsilon)^2}\left[\frac{5}{27}v_3 - \frac{t_3'}{16} + \frac{S_v}{T_0} - \frac{L}{3T_0} - \frac{1}{9}\right], \end{aligned} \tag{28}$$

and we can have $v_{1U} = v_1 - v_{1L}$ and $v_{2U} = v_2 - v_{2L}$.

A. Determination of $1+\epsilon$ power

We added in eq (6) the auxiliary density interaction with the $1+\epsilon$ power. We might regard $1+\epsilon$ as the many-body effect—for example, a three-body force if $\epsilon > \frac{1}{2}$. It is known, however, that interactions among more than three-bodies are unimportant in dense matter. Thus we might restrict the ϵ to be less than $\frac{1}{2}$. As the ϵ changes, the t_3 parameter changes sign which means the three-body force can be attractive or repulsive. In the general Skyrme model with the three-body force, the t_3 parameter is positive. We choose $\epsilon = 1/6$ so that the interaction has the form of $\rho_{t_1}^{7/6}\rho_{t_2}^{7/6}$. In zero-temperature, uniform matter, we have $u^{7/3}$ terms in the energy density. From eq. (19), the energy density has $u^{5/3}$, u^2, $u^{7/3}$, $u^{8/3}$, and u^3 terms if we have $\epsilon = 1/6$ so we can use a statistical approach in uniform matter. Fig 1. shows the energy per baryon from GNDF and APR[11] EOS. We can see that as the density increases, the pressure from the two models agrees very well.

B. The effective range of the nuclear force : r_0

In the Gaussian-interaction model, we can see the effective range of the force is given by r_0, which is approximately $\sim$ 1 to 2 fm. We don't have an analytic form of r_0, so we need

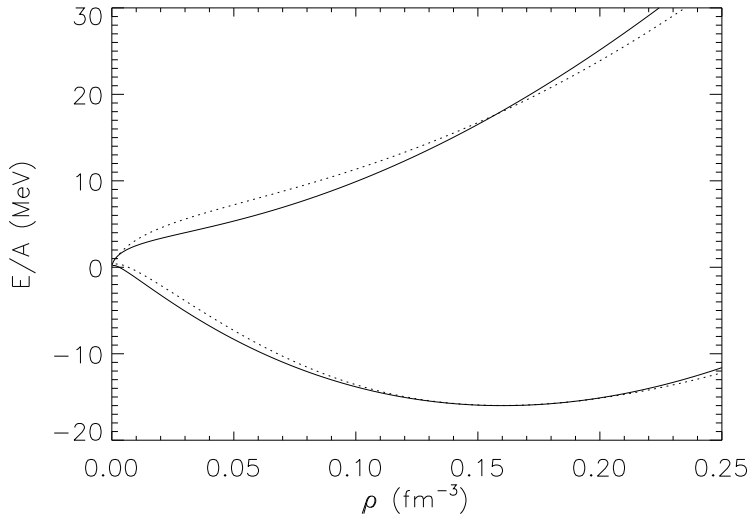

FIG. 1: The solid line represents the enery per baryon (uniform matter) using GNDF. The upper (lower) curve represents the energy per baryon of pure neutron matter(symmetric nuclear matter). The energy per baryon (dotted line) from the APR[11] EOS was added for comparison.

to rely on the numerical solution of the surface tension of semi-infinite nuclear matter:

$$\omega = \int_{-\infty}^{\infty} \big[\mathcal{E} - TS_n - TS_p - \mu_n\rho_n - \mu_p\rho_p + p_0\big]dz = -\int_{-\infty}^{\infty} \big[p(z) - p_0\big]dz\,, \tag{29}$$

where p_0 is the pressure at $z = -\infty$ or $z = +\infty$. In one-dimensional, semi-infinite nuclear matter, we assume that the nuclear density depends only on the z-axis; the Gaussian integral then becomes

$$\frac{1}{\pi^{3/2}r_0^3}\int d^3r\, u(r) = \frac{1}{\pi^{1/2}r_0}\int_{-\infty}^{+\infty} dz\, u(z)\,. \tag{30}$$

Experimental values of surface tension and surface thickness are $\omega = 1.250$MeV fm^{-2} and $t_{90-10} = 2.3$fm. Fig.2 shows the numerical calculation, which says that $r_0 = 1.205$fm from the surface tension and $r_0 = 1.149$ from t_{90-10} thickness. There is a 5% discrepancy between the two results. Table 1 shows the interaction parameters which we use in this paper when $K = 265$MeV, $S_v = 28$MeV, $L = 54$MeV, and $\epsilon = 1/6$. The simple density dependent interactions ($v_{1L,U}$) are attractive, on the other hand, the auxiliary density dependent interactions ($v_{2L,U}$), momentum dependent ineractions ($v_{3L,U}$) three-body force(t_3) are repulsive in our model.

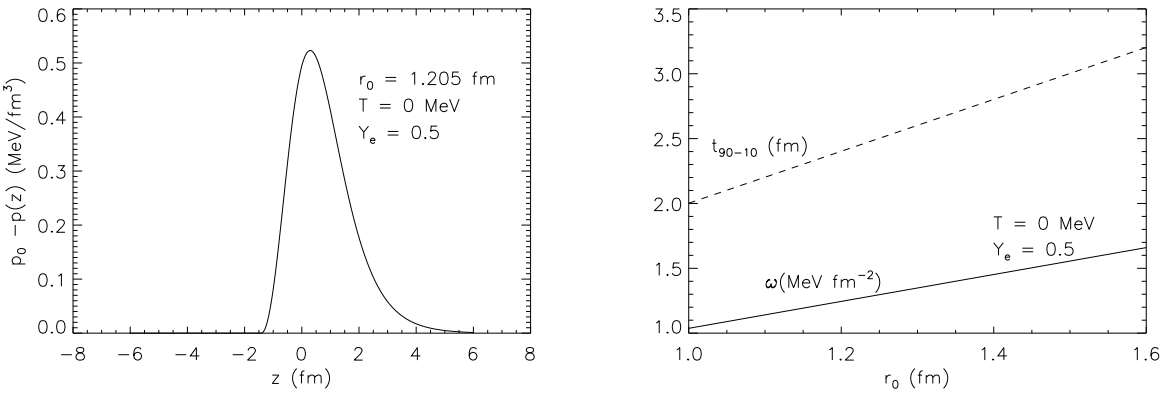

FIG. 2: The left figure shows the quantity $p_0 - p(z)$ at the semi-infinite nuclear surface when $r_0 = 1.205$fm and $\mathrm{Y}_e = 0.5$. The surface tension from this configuration is $\omega = 1.250$MeV fm^{-2}. The right figure shows the surface tension (solid line) and t_{90-10} thickness (dashed line) as a function of r_0. When $r_0 = 1.205$, $t_{90-10} = 2.412$fm. The surface tension and t_{90-10} thickness are both linear functions of r_0.

IV. NUCLEAR MATTER AND NUCLEI

A. Specific heat

The specific heat of uniform nuclear matter can be obtained by

$$C_V = T\frac{\partial S}{\partial T}\bigg|_\rho = \frac{\partial E}{\partial T}\bigg|_\rho . \tag{31}$$

For a non-interacting Fermion gas, the specific heat increases linearly with temperature. When the temperature is low enough, we expect that the specific heat of the nuclear matter tends to behave like a free Fermion gas. The specific heat formula for degenerate gas is given by[8]

$$C_V = \frac{1}{3}m^* k_F k_B^2 T\,, \tag{32}$$

where m^* is effective mass of a nucleon, k_F is the Fermi momentum, and k_B is Boltzman constant.

However, as the temperature increases, the non-linear behavior of the specific heat comes out so the degenerate gas formula is no longer valid, since the nucleons deep inside the Fermi surface are excited.

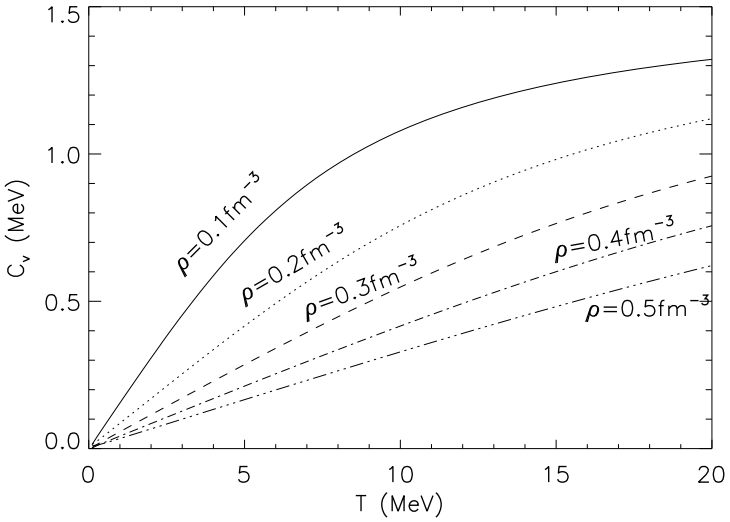

FIG. 3: This figure shows the specific heat per nucleon of uniform matter for different densities. If the temperature is low enough, the specific heat behaves linearly with temperature.

To calculate the specific heat of uniform nuclear matter, we use the Johns, Ellis, and Lattimer (JEL) method [21], which enables us to get the pressure, energy density and entropy density for a given degeneracy parameter. Fig.3 shows the specific heat per nucleon of uniform nuclear matter. It shows the linear relation between the specfic heat and temperature at low temperation as in eq. (32).

A detailed calculation of the specific heat at sub nuclear density in the neutron star needs to take into account the beta-equilibrium condition and heavy nuclei with a neutron gas. The specific heat plays an important role in the cooling process of neutron stars. In the neutron star crust, there are heavy nuclei and a free-neutron gas. The effective masses of protons and neutrons are different from the center of the heavy nuclei and dilute neutron gas, so we can't use eq. (32). In this case the specific heat at the neutron star crust can be calculated numerically by changing temperature and comparing the total energy change.

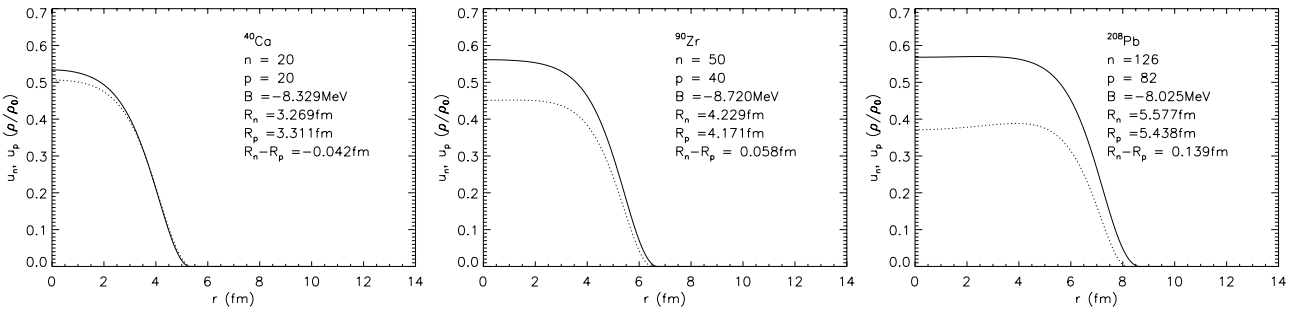

FIG. 4: This figure shows the basic properties of the closed-shell nuclei which can be obtained from the GNDF. The solid (dotted) line indicates the neutron (proton) density as a function of radius. As the number of nucelons in the nuclei increase, the neutron skin thickness($R_n - R_p$) increases.

B. Nuclei at $T = 0$ MeV

We can use the GNDF theory and the Lagrange multiplier method to find the radius and binding energy per nucleon for a single nucleus using the Winger-Seitz cell method. In the Lagrange multiplier method, the chemical potentials of protons and neutrons are constant in the Wigner-Seitz cell to minimize the total free energy. Fig. 4 shows the radius and binding energy of the closed-shell nuclei using this method. These results agree well with experiment[13]. ^{40}Ca has a larger charge radius than neutron radius because of the Coulomb repulsion between protons. The solid (dotted) line denotes neutron (proton) density. As the atomic number increases, the central density of neutrons increases; on the other hand the central density of protons decreases. The difference between charge and neutron radii increases and the neutron skin becomes thicker as the atomic number increases. In ^{208}Pb nuclei, the central density of protons is lower than the proton density of the outer part of nuclei ($r = 4 - 5$ fm) because of proton Coulomb repulsion.

Table II shows the proton and neutron radii and binding energy per baryon of closed shell nuclei from various nuclear models. The calculation from GNDF theory agrees well with experimental results.

TABLE II: Comparsion of the results from Steiner (Potential & Field Theoretical) et al.[13] , FRTF I[1], FRTF II[2] and the GNDF

Nucleus	Property	Experiment	Potential	FT	FRTF I	FRTF II	GNDF
^{208}Pb	r_{ch} (fm)	5.50	5.41	5.41	5.38	5.45	5.44
	BE/A(MeV)	7.87	7.87	7.77	8.01	8.17	8.02
	δR(fm)	0.12 $\pm$ 0.05	0.19	0.20	0.15	0.13	0.14
		0.20 $\pm$ 0.04					
^{90}Zr	r_{ch} (fm)	4.27	4.18	4.17	4.10	4.15	4.17
	BE/A(MeV)	8.71	8.88	8.65	8.77	9.00	8.72
	δR(fm)	0.09 $\pm$ 0.07	0.075	0.093	0.064	0.054	0.057
^{40}Ca	r_{ch} (fm)	3.48	3.40	3.34	3.22	3.26	3.31
	BE/A(MeV)	8.45	8.89	8.61	8.47	8.77	8.33
	δR(fm)	-0.06 $\pm$ 0.05	-0.044	-0.046	-0.036	-0.039	-0.042
		-0.05 $\pm$ 0.04					

C. Heavy nuclei in the neutron star crust

In the neutron star crust, heavy nuclei are formed with a free-neutron gas. These heavy nuclei are suspected to form a BCC (body centered cubic) structure. In the static equilibrium state, we calculate the density profile of heavy nuclei with a neutron gas using the Wigner-Seitz Cell method. The plot on the left side of Fig. 5 shows the proton (dotted line) and neutron density (solid line) profiles from the center (r=0 fm) of heavy nuclei when $\rho = 0.01\text{fm}^{-3}$. There are dripped neutrons outside of the heavy nuclei. The cell size (Rc), which is a rough estimate of the distance between neighboring heavy nuclei, is determined by nuclear density and beta equilibrium conditions ($\mu_n = \mu_p + \mu_e$). There is a wave function overlap at the boundary of Wigner-Setiz cell. The actual distance between heavy nuclei is $(8\pi/3)^{1/3}$Rc. The right side of Fig. 5 shows the binding energy per baryon as a function of Wigner-Seitz cell size. As the density decreases, the cell size increases and the energy per baryon converges to -8.0 MeV.

Table III shows the thermodynamic properties and physical dimensions of nuclei in the

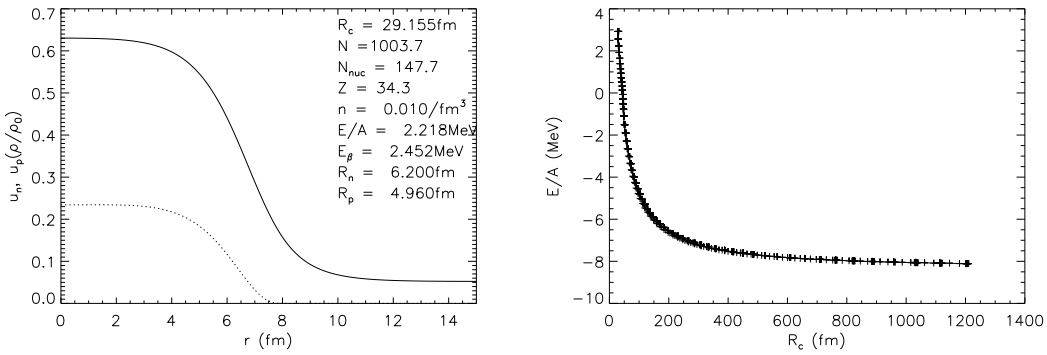

FIG. 5: In a neutron star, heavy nuclei exist. The left figure shows the density profile of proton (dotted line) and neutron (solid line). $r = 0$ fm means the center of heavy nuclei. Outside the heavy nuclei, there are dripped neutrons. As density decreases, the cell size increases and the energy per baryon converges to -8.0 MeV.

TABLE III: Nuclear properties in the neutron star crust

ρ (fm^3)	p (MeV/fm^3)	ϵ (MeV/fm^3)	N_{nuc}	Z	Rc (fm)
5.623×10^{-2}	0.181	53.06	271.6	89.51	25.12
5.012×10^{-2}	0.147	47.27	218.0	32.18	18.70
3.981×10^{-2}	9.332×10^{-2}	37.52	137.8	21.69	18.06
2.512×10^{-2}	3.965×10^{-2}	23.65	145.3	27.93	22.77
1.585×10^{-2}	1.976×10^{-2}	14.91	150.7	32.07	26.36
1×10^{-2}	1.081×10^{-2}	9.405	147.7	34.29	29.15
1×10^{-3}	7.988×10^{-4}	9.383×10^{-1}	116.3	38.50	40.71
1×10^{-4}	6.945×10^{-5}	9.352×10^{-2}	79.23	38.31	65.47
1×10^{-5}	1.480×10^{-6}	9.326×10^{-3}	58.02	36.98	131.4
1×10^{-6}	2.362×10^{-9}	9.311×10^{-4}	47.90	35.14	270.6
1×10^{-7}	1.714×10^{-9}	9.303×10^{-5}	43.37	34.10	569.7

neutron star crust. N_{nuc} and Z are number of neutrons and protons of heavy nuclei in the Wigner-Seitz Cell. The atomic number of heavy nuclei remains $Z \sim 35$ for a large range of densities before the phase transition to uniform matter. This means that the proton fraction decreases as the density increases. For a narrow range of densities, the atomic number

suddenly increases and the heavy nuclei merge with free neutrons to make uniform nuclear matter.

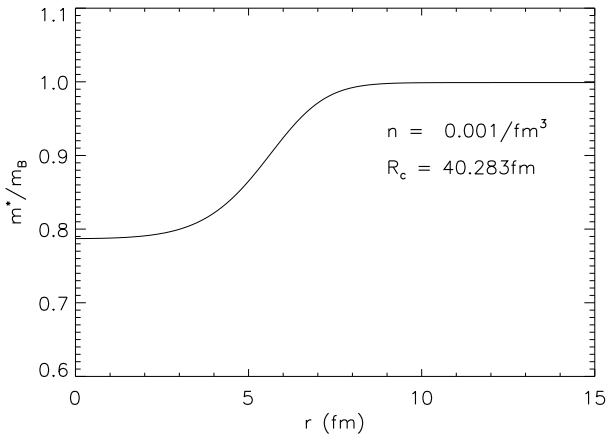

FIG. 6: Effective mass of nucleons in the Wigner-Seitz cell as a function of radial distance from the center of heavy nuclei. Since the nuclear interaction is weak at the boundary of the cell, the effective mass of nucleon and the pure mass of a nucleon become equal.

Fig. 6 shows the effective mass of nucleons in the Wigner-Seitz cell. The effective mass of nucleons in the Wigner-Seitz cell is given by eq. (13) and eq. (20),

$$m_t^* = \frac{m}{1 + \frac{5}{3}\left(v_{3L}\frac{\tilde{\rho_t}}{\rho_0} + v_{3U}\frac{\tilde{\rho_{t'}}}{\rho_0}\right)}\,. \tag{33}$$

Since we assume the momentum interaction is blind with respect to isospin, the effective mass is identical for different isospin nucleons. The effective mass to pure mass ratio of nucleons is 0.78 at the center of the heavy nuclei and becomes 1 at the outer region of the Wigner-Seitz cells since the density of nuclear matter is low at the outside of the heavy nuclei, the interaction energy of nuclear matter is weak.

V. PHASE TRANSITION

In the neutron star, we can see two types of phase transitions: one is the phase transition from nuclei with a neutron gas to uniform matter, and the other is the phase transition from

uniform nuclear matter to quark matter. During the first phase transition, we can see the nuclear pasta phase. That is, spherical nuclei become ellipsoidal, then cylindrical, and finally slab phase before nuclear matter becomes uniform matter. However, the energy difference is quite small, so that the effects on the large scale physics are neglible. On the other hand, the second phase transition is quite dramatic. The energy and pressure change significantly from nuclear matter to quark matter.

A. Uniform matter

To check the phase transition points from heavy nuclei with a neutron gas to uniform nuclear matter, we can simply compare the energy per baryon of uniform nuclear matter with the energy per baryon of nuclei with a neutron gas since the nuclear matter exists in the lowest energy states. The energy per baryon in uniform matter can be easily obtained by changing the '$\langle \dots \rangle$' integrals to non integral form from eq. (12) since the Gaussian integrations in uniform matter become unity. Typically there is a phase transition around $0.5\rho_0$. We know that in the outer crust of the neutron star the nuclei has a BCC structure. If we assume that the pasta phase exists in the low-density region, we may use the density perturbation to see the phase transition from nuclei with a neutron gas to uniform nuclear matter. We use the wave number pertubation to see the energy exchange, which has contributions from the volume effects, gradient effects, and Coulomb energy can be approximated[10],

$$v(q) \simeq v_0 + \beta q^2 + \frac{4\pi e^2}{q^2 + k_{TF}^2}\,, \tag{34}$$

where q is the sinusoidal variation of the wave number in the spatially periodic density perturbation.

The volume term is given by

$$v_0 = \frac{\partial \mu_p}{\partial \rho_p} - \frac{(\partial \mu_p/\partial \rho_n)^2}{(\partial \mu_n/\partial \rho_n)}\,. \tag{35}$$

The energy exchange from the gradient has the form

$$\beta = D_{pp} + 2D_{np}\xi + D_{nn}\xi^2\,, \quad \xi = -\frac{\partial \mu_p/\partial \rho_n}{\partial \mu_n/\partial \rho_n} \tag{36}$$

where the coefficients of the gradient terms are given by $D_{pp} = D_{np} = D_{nn} = 132\text{MeV} \cdot \text{fm}^5$[17]. The k_{TF} in the Coulomb interaction represents the inverse Thomas-Fermi screening

length of the electrons. When we see the change in the sign of v, the uniform matter phase is more stable than the perodic structure of the nuclei. The v has a minimum at

$$v_{min} = v_0 + 2(4\pi e^2\beta)^{1/2} - \beta k_{TF}^2\,, \tag{37}$$

when $q_{min}^2 = (4\pi e^2/\beta)^{1/2} - k_{TF}^2$.

Another way to see the phase transition is to use the thermodynamic instability. The thermodynamic stability condition can be described using the inequalities[14][17],

$$\begin{aligned} -\left(\frac{\partial P}{\partial v}\right)_\mu &> 0, \\ -\left(\frac{\partial \mu}{\partial q_c}\right)_v &> 0. \end{aligned} \tag{38}$$

where $P = P_b + P_e$ is the total pressure from electrons and baryons and $\mu = \mu_n - \mu_p$ is the difference between the neutron and proton chemical potentials, which is the electron chemical potential in beta-stable matter. q_c is defined as $q_c = x_p - \rho_e/\rho$. Mathematically, the inequalities in eq. (38) show that the energy per baryon is convex. Eq. (38) can be verified to be [14][17]

$$\begin{aligned} -\left(\frac{\partial P}{\partial v}\right)_\mu &= \rho^2\left[2\rho\frac{\partial E(\rho,x_p)}{\partial\rho} + \rho^2\frac{\partial^2 E(\rho,x_p)}{\partial\rho^2} - \left(\frac{\partial^2 E(\rho,x_p)}{\partial\rho\partial x_p}\rho\right)^2 \Big/ \frac{\partial^2 E(\rho,x_p)}{\partial x_p^2}\right] > 0, \\ -\left(\frac{\partial \mu}{\partial q_c}\right)_v &= \left(\frac{\partial^2 E(\rho,x_p)}{\partial x_p^2}\right)^{-1} + \frac{\mu_e^2}{\pi^2\hbar^3\rho} > 0\,. \end{aligned} \tag{39}$$

The second of eq. (39) always holds, so the first will determine the phase transition in the neutron star crust. In Xu et al.[17], they use a simple equation to determine the instability using the thermodynamic relation,

$$\frac{2}{\rho}\frac{\partial E}{\partial\rho}\frac{\partial^2 E}{\partial x_p^2} + \frac{\partial^2 E}{\partial\rho^2}\frac{\partial^2 E}{\partial x_p^2} - \left(\frac{\partial^2 E}{\partial\rho\partial x_p}\right)^2 = \frac{\partial\mu_n}{\partial\rho_n}\frac{\partial\mu_p}{\partial\rho_p} - \left(\frac{\partial\mu_n}{\partial\rho_p}\right)^2. \tag{40}$$

Eq. (40) is equilivalent to the volume part of the thermodynamic perturbation eq. (35) method except that there is a $\partial\mu_n/\partial\rho_n$ difference. Comparing the two methods (pertubation and thermodynamic instability) shows the effects of the gradient and Coulomb terms in the pertubation method on the transition densities. Fig. 7 shows transtion densities using the perturbation method and thermodynamic instability. The perturbation method has a lower transition density ($0.355\rho_0$) than thermodynamic instibility method ($0.406\rho_0$).

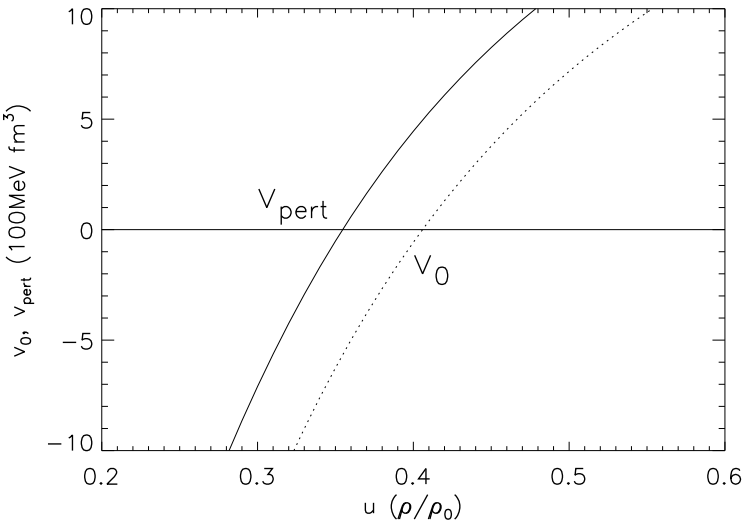

FIG. 7: We can see the transition density from nuclei with a neutron gas to nuclear matter. The solid line denotes the curve from the perturbation method. The dotted line corresponds to the thermodynamic instability method, equilivalent to v_0 in the perturbation method. The solid line has a transition density of $0.355\rho_0$ and the dotted line has a transition density of $0.406\rho_0$.

B. Quark matter

In this paper, we don't consider the appearance of hyperons since it is not clear how the hyperons and nucleons interact. Thus we simply consider the phase transition from uniform matter to quark matter. We use the MIT bag model for the quark matter equation of state. At T=0 MeV, the pressure and energy density are given by[7]

$$p = -B + \sum_f \frac{1}{4\pi^2(\hbar c)^3}\left[\mu_f(\mu_f^2 - m_f^2c^4)^{1/2}(\mu_f^2 - \frac{5}{2}m_f^2c^4) + \frac{3}{2}m_f^4c^8\ln\left(\frac{\mu_f + (\mu_f^2 - m_f^2c^4)^{1/2}}{m_fc^2}\right)\right]$$

$$\epsilon = B + \sum_f \frac{3}{4\pi^2(\hbar c)^3}\left[\mu_f(\mu_f^2 - m_f^2c^4)^{1/2}(\mu_f^2 - \frac{5}{2}m_f^2c^4) - \frac{1}{2}m_f^4c^8\ln\left(\frac{\mu_f + (\mu_f^2 - m_f^2c^4)^{1/2}}{m_fc^2}\right)\right], \tag{41}$$

where the density for each quark flavor is given by

$$\rho_f = \frac{(\mu_f^2 - m_f^2)^{3/2}}{\pi^2(\hbar c)^3}\,. \tag{42}$$

For the pure-quark phase we use $m_u = m_d = 0$, $m_s = 150$MeV and $B = 100$MeV fm^{-3}. In

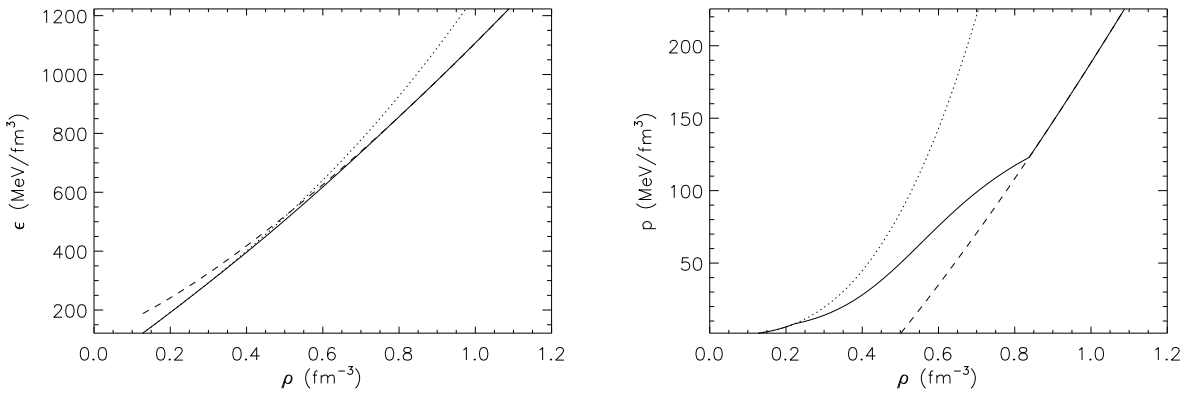

FIG. 8: The left panel shows the energy density of nuclear matter (dotted line), quark matter (dashed) and mixed phase (solid). The right panel shows the pressure of nuclear matter (dotted lined), quark matter (dashed) and mixed phase (solid).

the mixed phase of uniform nuclear matter and quark matter, we apply Gibb's conditions to minimize the free-energy density with two constraints, which are related to total number denstiy and charge neutrality.

$$\begin{aligned} \rho_b &= \chi\rho_N + (1-\chi)\rho_Q \\ Q &= \chi Q_N + (1-\chi)Q_Q = 0\,, \end{aligned} \tag{43}$$

where χ is the volume fraction of the uniform nuclear matter in the mixed phase and the subscript N (Q) represents nuclear (quark) matter. In the mixed phase, the total charge is globally neutral in contrast to pure nuclear matter and quark matter. From minimizing the free enegy, we have

$$\begin{aligned} p_N &= p_Q \\ \mu_n &= \mu_u + 2\mu_d \\ \mu_p &= 2\mu_u + \mu_d\,, \end{aligned} \tag{44}$$

then we have the energy density of the mixed phase

$$\epsilon = \chi\epsilon_N + (1-\chi)\epsilon_Q\,. \tag{45}$$

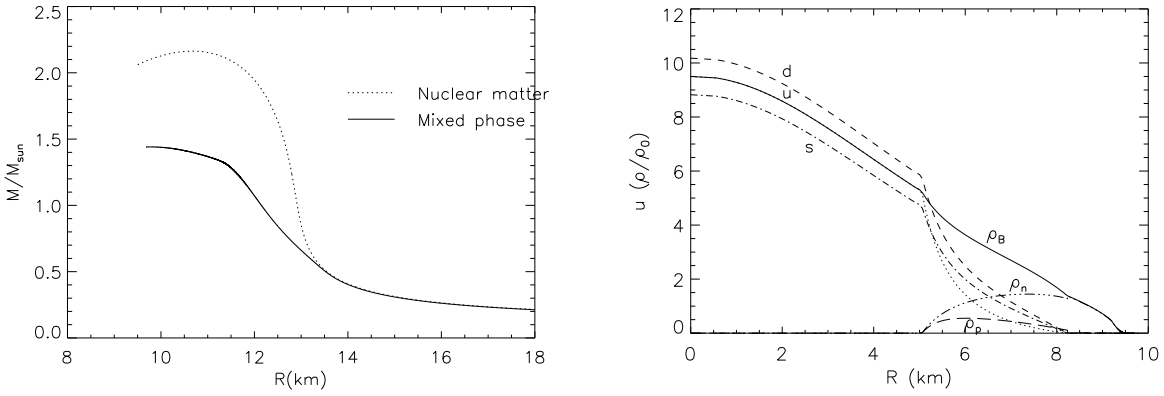

FIG. 9: The left panel shows the mass-radius relation of the neutron stars (dotted line) from the GNDF and the hybrid stars (solid line). The right panel shows the number density profile of a hybrid star which have M= 1.44M$_\odot$. At $r \sim 5.0$km, the phase transition to nuclear matter takes place, and protons and neutrons exit. When r=8.2km, the phase transition to nuclear matter is completed and there is no more quark matter.

As in the case of uniform matter, we assume beta-stable matter so that the chemical potentials of the nuclear matter and quark matter have the relation

$$\begin{aligned} \mu_n &= \mu_p + \mu_e \\ \mu_d &= \mu_s = \mu_u + \mu_e \,. \end{aligned} \tag{46}$$

Fig. 8 shows the energy density and pressure as a function of number density. The dotted (dashed) line represents nuclear (quark) matter. The solid line denotes the mixed phase.The phase transition begins when the baryon density becomes $1.386\rho_0$ and all nucleons turn into quark matter when the baryon density becomes $5.236\rho_0$.

If there is a phase transition in the core of a cold neutron star, the mass and radius are quite different from the case of a pure-nuclear-matter neutron star. The left panel of Fig. 9 shows the mass-radius relation of the neutron stars (dotted line) and hybrid stars (solid line). The right panel shows the number density profiles of a quark matter and nuclear matter of $1.44M_\odot$ hyrid star. The maximum mass of a cold neutron star with mixed phase (hybrid star) is 1.441M$_\odot$ and the central density of the neutron star is $9.585\rho_0$. The mass and radius curve with the mixed phase indicates when the mixed phase happens. As the distance from the center of the hybrid star increases, the phase transition to nuclear matter

takes place so that neutrons and protons appear($r \sim 5.0$km). Far from the center, the phase transition is completed ($r = 8.2$km); pure nuclear matter exists only for larger radii. The existence of quark matter in the hybrid star can be explained by angular momentum loss of the proto-neutron star. That is, fast-rotating neutron stars lose angular momentum because of magnetic dipole radiation; the central density of the neutron star increases due to the decrease in centripetal forec, then quark matter appears. Since quark matter has a lower energy density than pure nuclear matter, we might expect heating of the neutron star from latent heat from quark matter.

VI. ASTROPHYSICAL APPLICATION

A. Mass-radius relation of a cold neutron star

We know that the radius of a neutron star is $\sim$ 10km and the mass is $\sim 1.4 M_{\odot}$. In this system, the degeneracy pressure of the neutrons provides support against gravitational collapse. We can apply our model to calculate the mass and radius of neutron stars for a given central density. We use the Tolman-Oppenheimer-Volkov (TOV) equations which describe general relativistic hydrostatic equilibrium:

$$\begin{aligned} \frac{dp}{dr} &= -\frac{G(M(r) + 4\pi r^3 p/c^2)(\epsilon + p)}{r(r - 2GM(r)/c^2)c^2} \\ \frac{dM}{dr} &= 4\pi \frac{\epsilon}{c^2} r^2 \,. \end{aligned} \tag{47}$$

Fig. 10 shows the mass-radius relation for a cold neutron star. In the GNDF model, the maximum mass of a cold neutron star is 2.163$M_{\odot}$, and the correspoding radius is 10.673km. The maximum mass from the GNDF model is in between the FRTF truncated model (FRTF I) and the modified model of the FRTF (FRTF II)[1][2].

B. Moment of inertia of the neutron star

In the slow-motion approximation, the moment of inertia is given by[15]

$$I = \frac{8\pi}{3} \int_0^R r^4 (\rho + p) e^{(\lambda - \nu)/2} \omega \, dr \,, \tag{48}$$

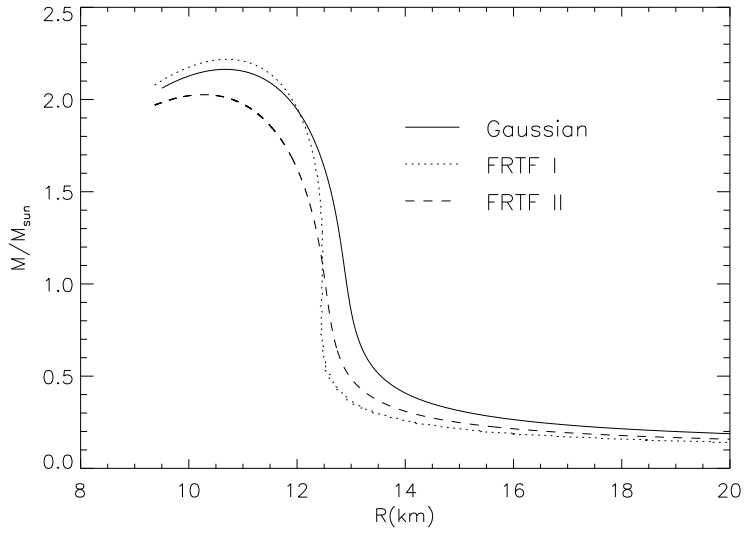

FIG. 10: Mass-radius relation for a cold neutron star. The mass of a cold neutron star from the Gaussian density functional model has a maximum mass of ($2.163 M_\odot$) when the central density is $6.74\rho_0$.

where $\lambda = -\ln(1-2m/r)$ and ν are the metric coefficients and ω is the rotational drag function. In terms of the function $j = e^{-(\lambda+\nu)/2}$, the rotational drag statisfies

$$\frac{d}{dr}\left(r^4 j \frac{d\omega}{dr}\right) = -4r^3\omega\frac{dj}{dr}\,, \tag{49}$$

with the boundary conditions

$$\omega_R = 1 - \frac{2I}{R^3}\,, \qquad \left(\frac{d\omega}{dr}\right)_0 = 0\,. \tag{50}$$

Therefore, the moment of inertia can be written as

$$I = -\frac{2}{3}\int_0^R r^3\omega\frac{dj}{dr}dr = \frac{1}{6}\int_0^R d\left(r^4\omega\frac{dj}{dr}\right) = \frac{R^4}{6}\frac{d\omega}{dr}\bigg|_R\,. \tag{51}$$

We note that the second-order differential equation that ω satisfies, eq. (49), can be instead written as a first order differential equation in terms of the function $\phi = d\ln\omega/d\ln r$,

$$\frac{d\phi}{dr} = -\frac{\phi}{r}(\phi+3) - (4+\phi)\frac{d\ln j}{dr}\,, \tag{52}$$

where

$$\frac{d\ln j}{dr} = -\frac{4\pi r^2}{r-2m}(\rho+p)\,, \tag{53}$$

with the boundary condition $\phi(0) = 0$. The moment of inertia becomes

$$I = \frac{R^3}{6}\phi_R\omega_R = \frac{\phi_R}{6}(R^3 - 2I)\,, \tag{54}$$

using the boundary condition for ω. This simplifies to

$$I = \frac{R^3\phi_R}{6 + 2\phi_R}\,. \tag{55}$$

Lattimer and Schutz proposed an empirical approximation for the moment of inertia[22],

$$I \simeq (0.237 \pm 0.008)MR^2\left[1 + 4.2\frac{M\mathrm{km}}{\mathrm{M}_\odot R} + 90\left(\frac{M\mathrm{km}}{\mathrm{M}_\odot R}\right)\right]. \tag{56}$$

Fig. 11 shows the moment of inertia of a cold neutron star. The color band represents upper and lower boundaries of the emprical approximation. FRTF I, II and GNDF agree quite well with this empirical approximation.

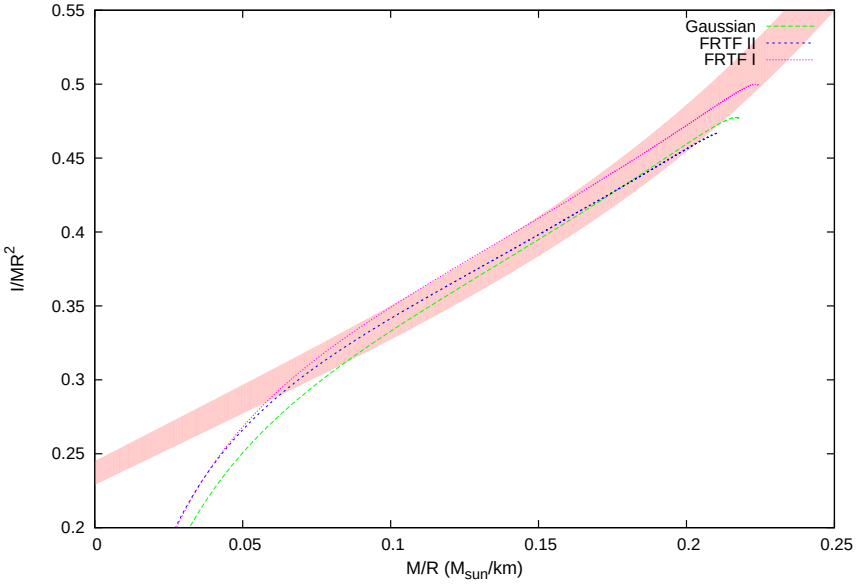

FIG. 11: Moment of inertia of a cold neutron star. The color band represents the upper and lower boundaries of the emprical approximation eq (56). Three different models show different curves; however, they represent the emprical results quite well.

C. Matter in the proto-neutron star

We expect that the core of a proto-neutron star is lepton rich ($Y_l \sim 0.4$) and the entropy per baryon is $s \sim 2-4$[23]. Since the Gaussian density functional model deals with non-relativistic nucleons, we use the relativistic leptonic formula to find the contribution from leptons to the total pressure, energy and entropy. Since the electrons and neutrinos are relativistic in proto-neutron star matter, we can get analytic solutions for leptons which are[3]

$$\mu_l = r - \frac{q}{r}\,, \quad r = [\sqrt{q^3+t^2}+t]^{1/3} \tag{57}$$

where $t = 3\pi^2(\hbar c)^3 n Y_l/g_l$ and $q = \frac{1}{3}(\pi T)^2 - \frac{1}{2}m_l^2c^4$. Here g_l is the spin degeneracy; thus $g_e = 2$, and $g_\nu = 1$ since the neutrino is only left handed. We assume that the neutrino is massless.

Expressions for the pressure and entropy per baryon are

$$\begin{aligned} p_l =& \frac{g_l\mu_l}{24\pi^2}\left(\frac{\mu_l}{\hbar c}\right)^3\left[1+\frac{2\pi^2T^2-3m_l^2c^4}{\mu_l^2}+\frac{\pi^2T^2}{\mu_l^4}\left(\frac{7}{15}\pi^2T^2-\frac{1}{2}m_l^2c^4\right)\right], \\ s_l =& \frac{g_lT\mu_l^2}{6n(\hbar c)^3}\left[1+\frac{1}{\mu_l^2}\left(\frac{7}{15}\pi^2T^2-\frac{1}{2}m_l^2c^4\right)\right]. \end{aligned} \tag{58}$$

To simplify the model of the core of a proto-neutron star, we assume that there are only protons, neutrons, electrons and electron neutrinos . In this case

$$\begin{aligned} s_t =& \quad s_n + s_p + s_e + s_{\nu_e} \\ Y_l =& \qquad\qquad Y_e + Y_{\nu_e}\,. \end{aligned} \tag{59}$$

If the core of the proto neutron star is in equilibrium (to be more exact, it is in quasi-static equilibrium), then the EOS needs to meet eq. (58) and eq. (59). On the other hand, in the cold, catalysed neutron star matter, we can simply say that there are only electrons. Thus

$$\mu_n = \mu_e + \mu_p\,. \tag{60}$$

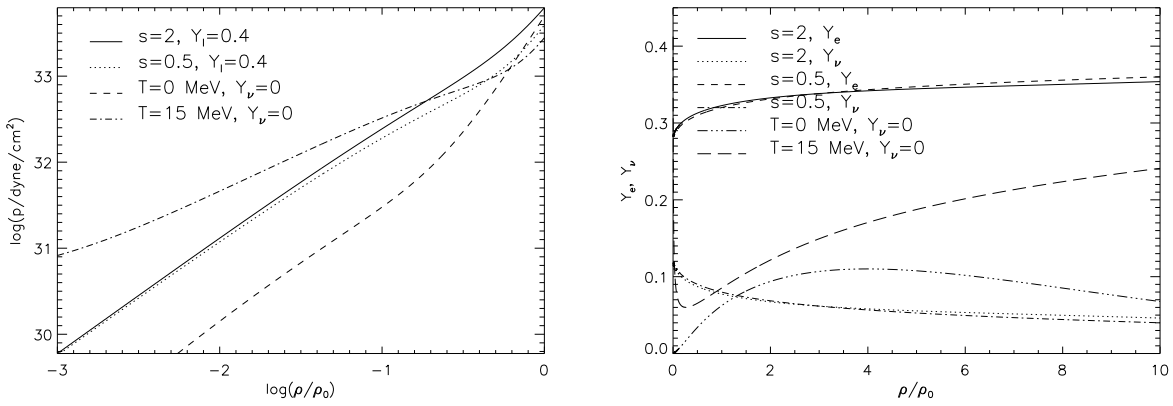

FIG. 12: The left figure shows the total pressure when s=2.0, s=0.5, T=0MeV and T=15MeV. The total pressure from various conditions shows different aspects. The total pressure for a fixed entropy per baryon (s=2, s=0.5) with fixed lepton fraction (Y_l=0.4) shows identical results for lower densities, but they have different behavior as the density increases. The temperature for a fixed entropy per baryon can be obtained from beta-equilibrium. The right figure shows the lepton fraction for four different cases. The results from fixed s=2 and s=4 are not distinguishable. The lepton fraction for T=0 and 15MeV, we assume beta-equilibrium.

If the interation of leptons with nuclear matter is weak, then the chemical potential and pressure of the leptons at zero temperature are given by[3],

$$\mu_l = \sqrt{(m_l c^2)^2 + (\hbar c)^2 (3\pi^2 \rho Y_l)^{2/3}}$$
$$p_l = \frac{1}{3\pi^2\hbar^3}\left[\sqrt{m^2c^4 + p_f^2 c^2}\left(-\frac{3}{8}m^2 p_f c^5 + \frac{p_f^3 c^3}{4}\right) + \frac{3}{8}m^4 c^8 \ln\Big(\frac{p_f c + \sqrt{m^2c^4 + p_f^2 c^2}}{mc^2}\Big)\right]. \tag{61}$$

In Fig. 12, the pressure is indistinguishable when s=2 and s=0.5 with fixed lepton fraction ($Y_l = 0.4$) at lower densities. However, for higher densities, they show a different behavior. At low densities, the pressure at high T is greater than the ones from the fixed entropy per baryon with fixed lepton fraction, however, at high densities, the pressure contribution from the trapped neutrinos is much more important than the thermal effect. The right side of Fig. 12 shows the lepton fraction from electrons and neutrinos for a given entropy per baryon. The lepton fraction for each case is almost identical. For the cases T=0 and 15 MeV, we assumed the beta-equilibrium condition. The electron fraction when T=15MeV increases from 0.06 to 0.25 between $\rho = 0.3\rho_0 < \rho = 10\rho_0$. Fig. 13 shows the various

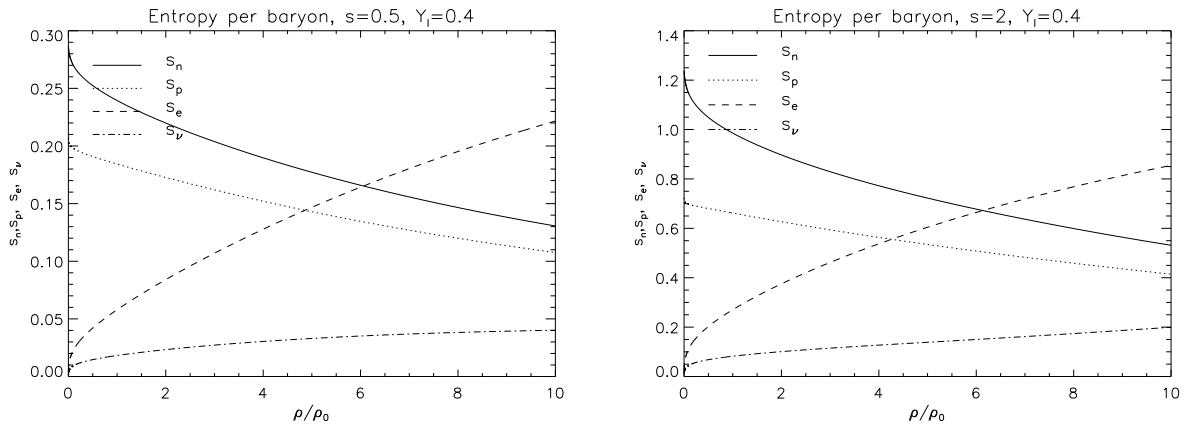

FIG. 13: Entropy contribution from baryons and leptons for each fixed entropy per baryon. Since the neutron (electron) fraction is always greater than the proton (neutrino) fraction, the entropy contribution from neutrons (electrons) is greater than protons (neutrinos).

entropy contribution for a given entropy per baryon and lepton fraction. Each graph shows the same trends. The entropy contributions from baryons is decreasing as baryon density decreases, and the electron's (neutron's) contribution to entropy is always greater than the neutrino's (proton's) contribution since the electron (neutron) fraction is greater than the neutrino (proton) fraction.

VII. CONCLUSIONS

In the GNDF model, the total energy consists of the kinetic energy, the finite-range effect, the zero-range effect, and the Coulomb energy. Using the Lagrange multiplier method, we find the potential energy, pressure, chemical potential and thermodynamic properties. The interaction parameters were obtained from the properties of infinite nuclear matter. We can find the charge radius and binding energy per baryon of the closed-shell nuclei. The Wigner-Seitz cell size increases as the density decreases and the binding energy per baryon approaches -8.0MeV. The effective mass becomes $0.78m$ at the center of the heavy nuclei and becomes m outside of heavy nuclei. We were also able to find the pressure of uniform symmetric nuclear matter and neutron matter. For finite temperature, we can see the specific heat of nuclear matter follows the general trend of the free fermions. Thus

the GNDF model is a good nuclear matter model to study for both low and high nuclear densities. We can improve the current model if we have more exact experimental results and we add additional interaction terms to explain the experimental results. The phase transition was studied using the GNDF model. The density perturbation suggested that the phase transition from non-uniform nuclear matter to uniform matter takes place at densities less than $0.5\rho_0$. When we take into account the phase transition from uniform nuclear matter to quark matter, we see there is a drastic change in the maximum mass of a neutron star, since the pressure and energy density of quark matter are significantly different from nuclear matter. The maximum mass of the hybrid star is less than $1.5M_\odot$. This might rule out the coexistence of nuclear matter and quark matter in compact stars. The GNDF model can be used to study proto-neutron star matter combined with a leptonic environment. Using the GNDF theory, we may compare the maximum and minimum masses of proto-neutron stars.

In a subsequent paper, we will study the nuclear pasta phase (spherical shell, cylinder, and slab geometry) using GNDF.

VIII. ACKNOWLEDGEMENTS

The author would like to thank James. M. Lattimer for useful discussion. This work was supported in part by US DOE grant DE-FG02-87ER40317.

---

[1] Y. Lim and J.M. Lattimer, *Finite-Range Thomas-Fermi Nuclear model I : the truncated model*, to be published.

[2] Y. Lim and J.M. Lattimer, *Finite-Range Thomas-Fermi Nuclear model II : the modified model*, to be published.

[3] J.M. Lattimer and F.D. Swesty, Nucl. Phys. A 535 (1991) 331.

[4] J.M. Lattimer, C.J. Pethick, D.G. Ravenhall and D.Q. Lamb, Nucl. Phys. A 432 (1985) 646.

[5] W. Greiner and J.A. Maruhn, *Nucler models*(Springer, 1989)

[6] S.L. Shapiro and S.A. Teukolsky, *Black holes, White Dwarfs, and Neutron Stars*(Wiley-interscience, 1983)

[7] N.K. Glendenning *Compact stars*(Springer, 2nd Edition)

[8] J.W. Negele and H. Orland *Quantum Many-Particle Systems* (Addison-Wesley, 1987)

[9] M. Baldo, P. Shuck, and X. Vinas, Phys. Lett. B 663 (2008) 390

[10] C.J. Pethick and D.G. Ravenhall, Ann. Rev. Nucl. Part. Sci. 45 (1995) 429

[11] A. Akmal, V. R. Pandharipande, and D. G. Ravenhall, Phys. Rev. C 58 (1998) 1804

[12] W.R. Gibbs and J.-P. Dedonder, Phys. Rev. C 46 (1992), p. 1825

[13] A.W. Steiner, M. Prakash, J.M. Lattimer and P.J. Ellis, Phys. Rep. 411 (2005) 325

[14] J.M. Lattimer and M. Prakash, Phys. Rep. 442 (2007) 109

[15] J.M. Lattimer, *Personal note*

[16] H.B. Callen, *Thermodynamics and An Introduction to Thermostatistics, 2nd Edition*(John Wiley & Sons, New York, 1985).

[17] J. Xu, L.W. Chen, B.A. Li, and H.R. Ma, Phys. Rev. C 79 (2009) 035802

[18] N.K. Glendenning, Phys. Rev. D 46 (1992) 1274

[19] M. Prakash, J.R. Cooke, and J.M. Lattimer, Phys. Rev. D 52 (1995) 661

[20] W.H. Press, S.A. Teukolsky, W.T. Vetterling, and B.P. Flannery, *Numerical recipes in Fortran 77, 2nd Editon*(Cambridge, 1995)

[21] S.M. Johns, P.J. Ellis, and J.M. Lattimer, ApJ 473 (1996) 1020

[22] J.M. Lattimer and B.F. Schutz, ApJ. 629 (2005) 979

[23] A. Burrows and J.M. Lattimer, ApJ. 307(1986) 178

[24] J. Macher and J.S. Bielich, Eur. J. Phys. 26 (2005) 341

[25] K. Oyamatsu, Nucl. Phys. A 561 (1993) 431

[26] G. Baym, H.A. Bethe, and C.J. Pethick, Nucl. Phys. A 175 (1971) 225

[27] G. Baym, C.J. Pethick, and P. Sutherland, Apj. 170 (1971) 299

[28] J.W. Negele and D. Vautherin, Nucl. Phys. A 207 (1973) 298

[29] P. Bonche and D. Vautherin, Nucl A 372 (1981) 496

[30] H. Shen, H. Toki, K. Oyamatsu and K. Sumiyoshi, Nucl A 721 (2003) 1048c

[31] G. Shen, C.J. Horowitz and S. Teige, Phys. Rev. C82(2010) 015806